

Dynamics of crosshatch patterns in heteroepitaxy

Fabrizio Rovaris,¹ Marvin H. Zoellner,² Peter Zaumseil,² Anna Marzegalli,¹ Luciana Di Gaspare,³ Monica De Seta,³ Thomas Schroeder,^{2,*} Peter Storck,⁴ Georg Schwalb,⁴ Giovanni Capellini,^{2,3} and Francesco Montalenti^{1,†}

¹*L-NESS and Department of Materials Science, University of Milano-Bicocca, Via Roberto Cozzi 55, I-20125 Milano, Italy*

²*IHP–Leibniz-Institut für innovative Mikroelektronik, Im Technologiepark 25, 15236 Frankfurt (Oder), Germany*

³*Dipartimento di Scienze, Università di Roma Tre, Viale Guglielmo Marconi, 446, 00146 Roma, Italy*

⁴*Siltronic AG, Hanns-Seidel-Platz 4, 81737 München, Germany*



(Received 14 March 2019; published 27 August 2019)

Regular surface undulations, called cross-hatch patterns, appearing at the free surface of lattice-mismatched heteroepitaxial films are a key signature of plastic relaxation. Here we show that the dynamics of cross-hatch formation is accurately described by a continuum model based on strain-mediated surface diffusion, provided that a realistic distribution of dislocations is considered. We demonstrate quantitative agreement between our time-dependent simulations and dedicated atomic force microscopy experiments on $\text{Si}_{0.92}\text{Ge}_{0.08}$ films grown on Si(001) at various thicknesses, finally shedding light on the origin and on the dynamical behavior of a widely investigated pattern, first observed more than half a century ago.

DOI: [10.1103/PhysRevB.100.085307](https://doi.org/10.1103/PhysRevB.100.085307)

I. INTRODUCTION

The advancement of the microelectronic industry has relied on the aggressive downscaling of the size typically featured by devices in the silicon-based complementary metal oxide semiconductor (CMOS) technology, known as the “more Moore” approach. However, since the “standard” MOS transistor architecture cannot be miniaturized beyond a certain size, the microelectronic industry has pursued different solutions, ranging from different transistor architectures (such as multiple gates [1], fin-FET [2], and gate-all around [3]) to the heterointegration of different semiconductors to be used as base material for *p*- and *n*-MOSFET channels [4] or as stressors for Si [5]. The possibility to heterointegrate advanced materials on Si substrates during the front end of the line stages of the manufacturing process has prompted a wealth of studies aiming at achieving high quality of the heterolayer while preserving its manufacturability in the Si foundries [6]. Two of the major issues that have to be addressed while attempting the integration of a different semiconductor on silicon are related to the difference of the thermal expansion, inducing a thermal strain, and to the different lattice parameter and symmetry featured by the epilayer and the substrate. The latter usually leads to a deformation of the epilayer lattice, i.e., heteroepitaxial strain, and/or to the formation of non-planar epilayers featuring a three-dimensional morphology not suitable for the fabrication of electronic devices [7]. The heteroepitaxial strain limits the maximum thickness that an epilayer can feature before its plastic relaxation, i.e., the loss of its in-plane lattice coherence with that of the substrate, through the formation of misfit dislocations (MD) [8]. The

formation of the so-called “cross-hatch” pattern (CHP) at the surface of the epilayer is a key signature of the occurrence of the plastic relaxation. The CHP, first observed half a century ago [9], is now recognized as a common feature for a broad range of heteroepitaxial systems such as InGaAs/GaAs [10], GaAsP/GaAs [11], GaAs/Si [12], SiGe/Si [13], and even IV-VI heteroepitaxial layers [14].

For the common case of growth on (001)-oriented fcc films, the resulting surface morphology is often (i.e., for low misfit, see below) particularly simple, featuring two arrays of lines oriented along two orthogonal [110]-equivalent directions. As this reflects the symmetry of the MD network [13], a link between the epilayer morphology and plastic relaxation could be easily argued. However, this one-to-one correlation of the CHP geometry with the MD network is far from being understood, with several experimental observations still remaining unclear. For instance, the distance between adjacent undulations of the CHP, which is not truly periodic, can be orders of magnitude larger than the average distance between dislocations [15]. Even the origin of the undulations is still debated. Both bunching of the surface steps produced by the nucleation and gliding of dislocation loops [15,16] and the redistribution of surface adatoms induced by inhomogeneities of the strain field at the free surface [17,18] have been proposed as the root cause for the CHP formation.

In this paper we address and clarify the origin and the dynamics of the CHP by providing a direct, quantitative, time-dependent comparison between a suitable continuum model and dedicated experiments on a low-misfit $\text{Si}_{1-x}\text{Ge}_x/\text{Si}(001)$ planar film.

The paper is organized as follows. In Sec. II our method is introduced, with Sec. II A dealing with the experimental procedure involved for the growth and characterization of the samples and Sec. II B introducing the theoretical model proposed to describe the dynamical evolution of the formation of CHP. Results follow in Sec. III, with a detailed comparison

*Present address: Leibniz Institut für Kristallzüchtung, Max-Born-Strasse 2, 12489 Berlin, Germany.

†francesco.montalenti@unimib.it

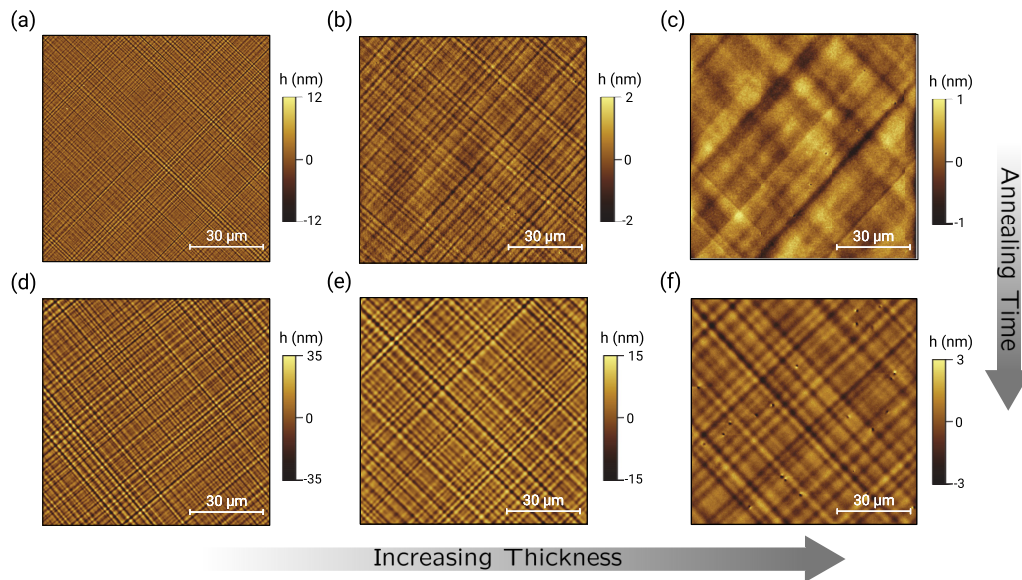


FIG. 1. Cross-hatch patterns. AFM images obtained for the three sample sets A, B, and C described in the text. (a)–(c) AFM after 10 min of annealing for the 600-, 1500-, and 3000-nm samples, respectively. (d)–(f) AFM after 60 min of annealing at 1050 °C.

between simulations and experimental results. Conclusions and final remarks are reported in Sec. IV.

II. METHOD

A. Experimental

A quantitative investigation of a CHP involves the estimation of different morphological parameters, such as the root-mean-square roughness ρ and the average distance between CHP undulations peaks λ . In general, such quantities depend on several variables, such as the deposition process parameters, the presence of one or more annealing steps, the lattice misfit, the degree of plastic relaxation, and the actual spatial distribution of MD, thus making the result interpretation non-trivial. Therefore, in this work we have designed experiments carefully, in order to analyze the influence of such quantities one at a time. Along this line, we have also minimized the complexity of the CHP by depositing films with a very low misfit f , fixing the Ge content at $x = 0.08$ ($f = 0.0032$). In fact, it is well known that the number of (semi-)loops in heteroepitaxial layers increases for larger misfit, eventually giving rise to highly entangled distributions of MD which, in turn, are associated with complex surface morphologies displaying no clear CHP. Finally, we investigated the surface morphology evolution using the annealing process (rather than during deposition), thereby reducing effects linked to the actual growth kinetics.

The dependence of the CHP on the annealing time (10 and 60 min) and on the film thickness was analyzed at a given relaxation degree, annealing temperature ($T = 1050$ °C), and (average) dislocation distribution. This was made possible by first growing, by means of a high-temperature chemical vapor deposition process [19], a set of very thick (3000 nm) samples, showing full plastic relaxation, as demonstrated by x-ray diffraction measurements. After the growth, we realized three sample sets: A, B, and C. A “gentle” chemical mechanical polishing (CMP) was used on group A, negligibly reducing

the film thickness (gentle CMP was done using a standard Si process, stopping the process after 10 s, corresponding to the removal of about 20 nm of the SiGe layer). Samples of group B (C), instead, were thinned down by CMP to a thickness of 1500 nm (600 nm). After the CMP process, the roughness of all the samples was in the sub-nanometer scale, allowing us to rule out any significant role played by step bunches initially present at the free surface in the subsequent evolution.

In Fig. 1 we display atomic force microscopy (AFM) images acquired on the various samples in tapping mode using a Bruker Dimension Icon setup equipped with a closed-loop scanner and using Bruker TESP-SS supersharp tips featuring a 2-nm nominal tip radius. A new tip was used for each individual sample investigated. The surface of all the samples presents a clear CHP, with two sets of perpendicular features aligned along two [110]-equivalent directions. This is interesting per se as CHPs have typically been observed only after growth. Here we demonstrate that even if one removes the CHP formed during growth, an annealing following the CMP restores the pattern. Actually, we show below that annealing after growth and annealing after growth + CMP lead to almost identical CHPs.

B. Model definition

The model proposed in this paper to describe the dynamical evolution of CHPs relies on a continuum 1 + 1D approach for the morphological evolution of plastically relaxed films, as introduced in Ref. [20]. This approach describes the surface evolution based on surface diffusion, with the flux of adatoms determined by the gradients in the surface chemical potential μ . The evolution of the surface profile h can be written, in the weak-slope approximation, by projecting the material flux along the vertical direction:

$$\frac{\partial h}{\partial t} = \nabla M \nabla_s \mu, \quad (1)$$

where M is the adatom mobility and the subscript “s” denotes the surface gradient operator.

The central quantity in Eq. (1) is the chemical potential which consists of two terms, $\mu = \mu_s + \mu_e$. The first one, μ_s , represents the energy cost associated with the formation of new free surfaces and, for isotropic surface energy density γ , is linearly proportional to the local surface curvature κ , $\mu_s \approx \kappa\gamma$ [21]. In the following simulations γ was set to $80 \text{ meV}/\text{\AA}^2$, typical of Si(001) [22]. The second term is proportional to the elastic energy density, which can be numerically evaluated by solving partial differential equations for the mechanical equilibrium using the finite element method (FEM) within the linear elasticity framework for isotropic solids. The introduction of the lattice misfit as well as the presence of dislocations in this approach is performed by means of the eigenstrain formalism [23]. This allows one to take into account dislocations with assigned Burgers vectors and positions (see Ref. [20] for further details) by defining an eigenstrain ε^* for the epitaxial film: $\varepsilon_{ij}^*(x, y) = f\delta_{ij} + \varepsilon_{ij}^d(x, y)$, where ε^d is the sum of the strain field associated with each individual defect, evaluated by means of analytical expressions [24]. The total strain used to compute the elastic energy will be then $\varepsilon = \frac{1}{2}(\nabla\mathbf{u} + \nabla\mathbf{u}^T) - \varepsilon^*$, with \mathbf{u} being the local displacement field obtained by the FEM solution for the elastic problem.

III. RESULTS AND DISCUSSION

In this section we apply the model described above to a 600-nm-thick $\text{Si}_{0.92}\text{Ge}_{0.08}/\text{Si}(001)$ film, corresponding to the system analyzed in Fig. 1. At first, we considered an array of 60° dislocations, the prevalent type of MD in the low-misfit SiGe/Si material system [25], located at the heterointerface, evenly spaced, and with identical Burgers vectors [see schematics in the bottom panel of Fig. 2(a)]. The dislocation-dislocation separation is fixed at $d \approx 70 \text{ nm}$, as

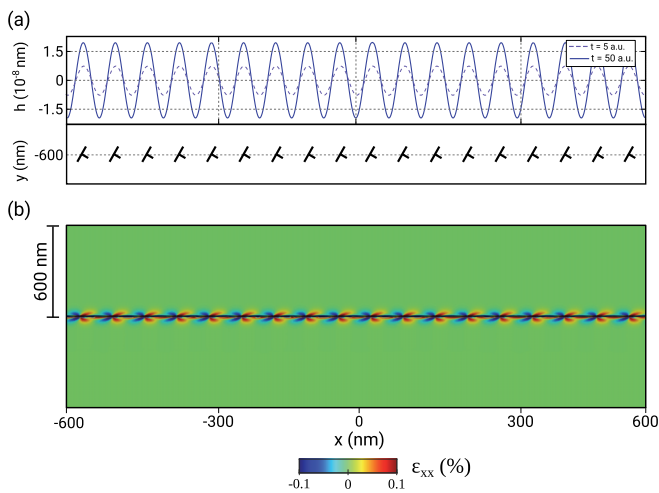


FIG. 2. Results for an ideal array of 60° dislocations. (a) Surface profile obtained after the annealing of the initially flat film for $t = 5$ a.u. and $t = 50$ a.u. The system has reached an equilibrium: the surface morphology does not evolve anymore upon further annealing. (b) Strain field (ε_{xx}) component resulting in a 600-nm-thick film relaxed by an ideal array of 60° dislocations.

required for the complete plastic relaxation of the strain. The simulation cell was set to $L = 1200 \text{ nm}$ and periodic boundary conditions were applied. The initial profile is taken to be perfectly flat, so that the only source of inhomogeneities in the chemical potential is due to the presence of the strain field associated with the network of MD itself, which generates a gradient in the chemical potential. The latter induces a deformation of the surface profile, which is controlled by the balance between elastic and surface energy. As can be observed in Fig. 2(a), undulations develop and evolve in time until the surface reaches a final equilibrium configuration. Under these ideal conditions the final periodicity matches the one of the underlying MD arrays [Fig. 2(b)]. This is in accordance with the static model of Ref. [18], but, evidently, not with the experimental observations of Fig. 1 where the average distance between subsequent undulations is almost 2 orders of magnitude larger, at the micrometer scale. We checked that the situation does not change if a second, ideal dislocation distribution is considered, consisting of a dislocation distribution where dislocations are still equispaced but the orientation of the Burgers vectors is alternated between the two directions available to relax the strain [25]. Notice that simulations not only predict the wrong periodicity they also strongly underestimate the roughness. Actually, the predicted value has no physical meaning, being much smaller than a single lattice parameter. In summary, Eq. (1) fails in predicting the experimental observations if an ideal distribution of dislocations is considered.

In a recent work (see Ref. [25] for details) a detailed analysis of the network of misfit dislocations for thin $\text{Si}_{0.92}\text{Ge}_{0.08}/\text{Si}$ was provided. The nearest-neighbor distance r distribution of the MDs can be very accurately reproduced by a log-normal distribution:

$$f(r) = \frac{1}{r\sqrt{2\pi}\sigma} \exp\left[-\frac{(\ln r - \log \alpha)^2}{2\sigma^2}\right]. \quad (2)$$

In Eq. (2) α represents the logarithm of the mean distance between adjacent MDs, controlling the degree of plastic relaxation introduced by the array of dislocations, while σ represents the dispersion of the distribution. This result, being in agreement with the one already reported in the literature by Kaganer *et al.* [16] for the study of the initial stages of relaxation of a $\text{Si}_{0.4}\text{Ge}_{0.6}/\text{Si}(001)$ system, suggests a possible general behavior. As a consequence we replaced, in the model, the ideal distribution with one extracted from Eq. (2), using the same σ value found in Ref. [25] ($\sigma = 0.7$) and fixing α based on the present dislocation-dislocation distance giving on average full relaxation of the SiGe film ($\log \alpha = 4.2$). The orientation of the individual Burgers vectors was randomly assigned, again following the results of Ref. [25].

Simulation results for the three different experimental thicknesses (600, 1500, and 3000 nm) and for different annealing times are reported in Fig. 3 [26]. It is evident that by considering a realistic distribution of dislocations both the typical roughness and the average separation between surface undulations become fully consistent with the experimental findings. Notice that the timescale in the simulations is controlled by the M value of Eq. (1), depending on T [27]. As all samples were annealed at the same temperature,

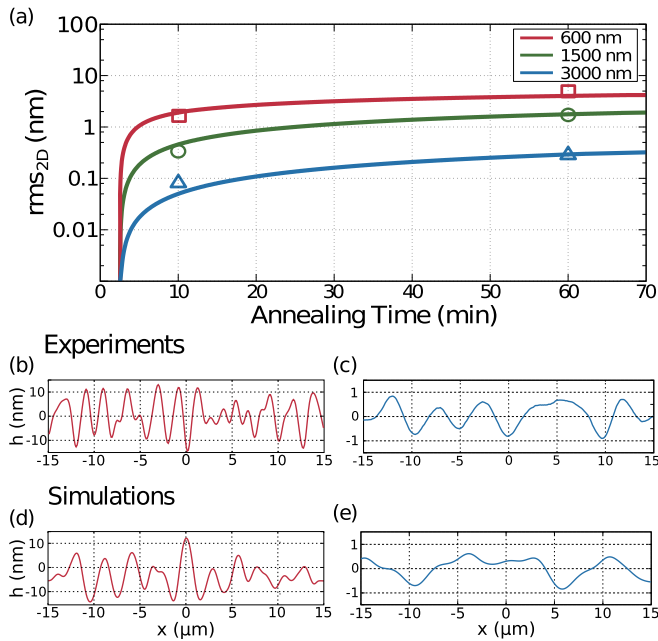


FIG. 3. Comparison between simulations and experimental results. (a) rms_{2D} [26] roughness evolution predicted by the simulations in solid lines and experimental results for the three sample groups A, B, and C (triangles, circles, and squares, respectively) after 10 and 60 min of annealing. The scan of the experimental surface profiles along one of the two $\langle 110 \rangle$ directions for the 600- and 3000-nm samples after 60 min of annealing are reported in panels (b) and (c) and the corresponding simulated profiles are shown in panels (d) and (e).

a single rescaling factor should be in principle sufficient to match experimental and simulation times. Indeed, we forced such matching using the two roughness points of the 1500-nm-thick sample and obtained all other results displayed in Fig. 3(a) with no further readjustment. The overall quantitative, time-dependent agreement between experimental data and simulations is excellent.

Having demonstrated the predictive power of the model, we can now exploit it to directly interpret the interesting physical behavior of the CHP. For instance, the lower ρ value observed for increasing film thickness is readily explained: the dynamics of CHP formation in the model is entirely determined by the magnitude of strain inhomogeneities at the free surface, which is obviously lowered by increasing the film thickness, when the sources of the strain field at the heterointerface get more “buried.”

Besides the value of the roughness, the other key quantity characterizing the CHP is the typical distance between surface undulations. In Figs. 3(b)–3(c) we report the surface profiles by AFM taken along one of the two equivalent $[110]$ CHP directions, for the 3000-nm-thick sample thinned down to 600 nm and the 3000-nm-thick sample after 60 min of annealing. This can be directly compared with the simulated profiles in panels Figs. 3(d) and 3(e) for the corresponding two film thicknesses. Albeit qualitatively, we can clearly see that our model correctly describes the increase of the typical distance between CHP peaks, related to the fading out of the strain field modulation induced by the MD network in a thicker epilayer.

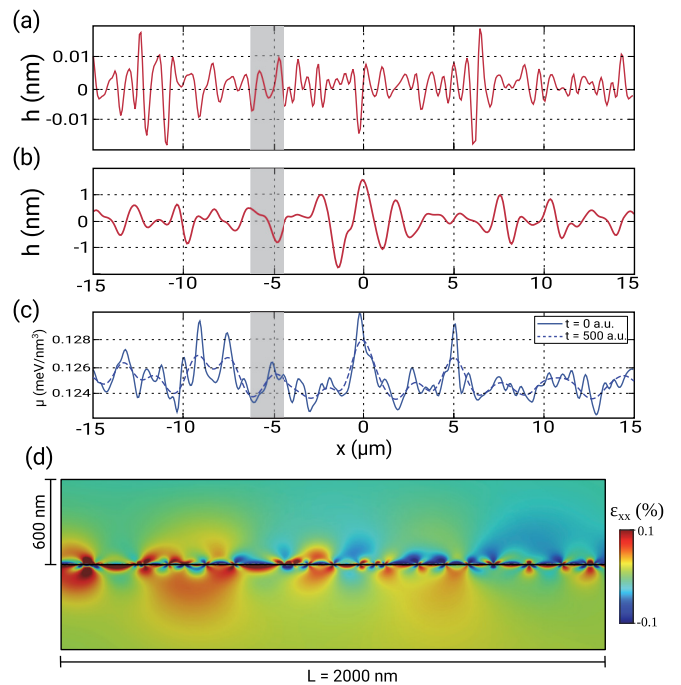


FIG. 4. Early stages of the surface roughness evolution for the 600-nm sample. Panels (a) and (b) show the surface profile obtained after the annealing of the initially flat film for $t = 1$ a.u. and $t = 500$ a.u. (c) Plot of the surface chemical potential μ after the same two annealing times. (d) Strain field (ϵ_{xx}) calculated in the same 2000-nm region shaded in panels (a)–(c).

The dynamics of the earlier stages of CHP formation for the 600-nm sample can be better appreciated by looking at Fig. 4. The initial response of the system consists of fast-growing high-frequency undulations [Fig. 4(a)] that tend to disappear in later stages of the evolution, when larger λ and larger amplitude oscillations develop, as shown in Fig. 4(b). This behavior is consistent with the evolution of the surface chemical potential μ presented in Fig. 4(c). Furthermore, we report in Fig. 4(d) the strain field produced by the MD network in the same 2- μm area shaded in Figs. 4(a)–4(c). The difference with respect to the ideal dislocation distribution can be easily appreciated by comparing it with Fig. 2(b). It is evident that the nonuniform distribution of the dislocation locations gives rise to superpositions of the strain field resulting in the more complex dynamical evolution of the surface profile, finding an equilibrium wavelength λ much larger than the dislocation-dislocation distance.

The above reported analysis was based on annealing of initially flat, fully relaxed epilayers. This procedure yields clear advantages. We notice, indeed, that CHPs in the literature are usually analyzed directly after growth. As a consequence the observed pattern corresponds to some unknown stages (depending on the deposition conditions) of evolution towards equilibrium, making it very hard to rationalize quantitative estimates in a broader context. Finally, we point out that, at variance with the thinning of the epilayer, the surface smoothing due to the CMP plays no real role in the subsequent evolution of the surface under annealing. This is shown in Fig. 5, where we compare an as-grown 600-nm-thick film

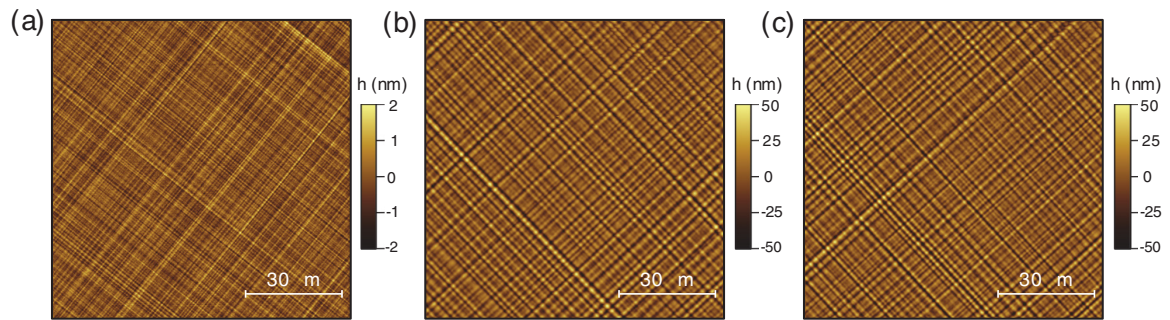


FIG. 5. Influence of CMP process. AFM images of 600-nm-thick $\text{Si}_{0.92}\text{Ge}_{0.08}$ samples: (a) as-grown reference sample, (b) sample after a 60-min annealing process at 1050°C , and (c) sample undertaking a gentle CMP before the same 60-min annealing process.

($\lambda = 1.3 \mu\text{m}$ and $\rho = 0.44 \text{ nm}$) [panel (a)] with its twin sample annealed for 60 min before [panel (b)] or after [panel (c)] undergoing a gentle CMP. The CHP in Figs. 5(b) and 5(c) is almost identical (same $\lambda = 2 \mu\text{m}$ and $\rho = 13.3$ and 13.6 nm , respectively), even from the quantitative point of view. Annealing is thus sufficient to provide a “universal evolution” of the CHP, erasing all possible memory of the evolution stages of the pattern during growth. With this respect, our results are of more general validity.

IV. CONCLUSION

In conclusion, in this paper we have shown that a two-dimensional (2D) continuum model based on strain-mediated surface diffusion predicts a dynamical evolution of the roughness of low-misfit heteroepitaxial films in good quantitative

agreement with experiments. This allows for a direct interpretation of the cross-hatch patterns, here linked to dishomogeneities in the dislocation distribution, half a century after their first observation. Despite being checked by comparison with a specific system, the model is general and is expected to describe a broad class of different (low-misfit) systems.

ACKNOWLEDGMENTS

This work is part of the TAPES3 project which received funding from the European Union’s Horizon 2020 research and innovation programme under Grant Agreement No. 783247 and the Ministry of Education and Research (BMBF) of Germany under Project No. 16ESE0293. The Lime Laboratory of Rome Tre University is acknowledged for technical support.

-
- [1] I. Ferain, C. A. Colinge, and J. P. Colinge, *Nature (London)* **479**, 310 (2011).
 - [2] C. Y. Chi, C. C. Chang, S. Hu, T. W. Yeh, S. B. Cronin, and P. D. Dapkus, *Nano Lett.* **13**, 2506 (2013).
 - [3] T. Vasen, P. Ramvall, A. Afzaljan, G. Doornbos, M. Holland, C. Thelander, K. A. Dick, L. E. Wernersson, and M. Passlack, *Sci. Rep.* **9**, 1 (2019).
 - [4] S. Takagi, S.-H. Kim, M. Yokoyama, R. Zhang, N. Taoka, Y. Urabe, T. Yasuda, H. Yamada, O. Ichikawa, N. Fukuhara, M. Hata, and M. Takenaka, *Solid-State Electron.* **88**, 2 (2013).
 - [5] O. G. Schmidt and K. Eberl, *IEEE Trans. Electron Devices* **48**, 1175 (2001).
 - [6] T. E. Kazior, *Philos. Trans. R. Soc., A* **372**, 20130105 (2014).
 - [7] D. J. Eaglesham and M. Cerullo, *Phys. Rev. Lett.* **64**, 1943 (1990).
 - [8] E. A. Fitzgerald, *Mater. Sci. Rep.* **7**, 87 (1991).
 - [9] R. A. Burmeister, G. P. Pighini, and P. E. Greene, *Trans. Metall. Soc. AIME* **245**, 587 (1969).
 - [10] K. H. Chang, R. Gilbala, D. J. Srolovitz, P. K. Bhattacharya, and J. F. Mansfield, *J. Appl. Phys.* **67**, 4093 (1990).
 - [11] S. Kishinû, M. Ogirima, and K. Kurata, *J. Electrochem. Soc.* **119**, 617 (1972).
 - [12] T. Nishioka, Y. Itoh, A. Yamamoto, and M. Yamaguchi, *Appl. Phys. Lett.* **51**, 1928 (1987).
 - [13] E. A. Fitzgerald, Y. H. Xie, D. Monroe, P. J. Silverman, J. M. Kuo, A. R. Kortan, and F. A. Thiel, *J. Vac. Sci. Technol. B* **10**, 1807 (1992).
 - [14] G. Springholz, *Appl. Phys. Lett.* **75**, 3099 (1999).
 - [15] A. M. Andrews, J. S. Speck, A. E. Romanov, M. Bobeth, and W. Pompe, *J. Appl. Phys.* **91**, 1933 (2002).
 - [16] V. Kaganer, T. Ulyanenkova, A. Benediktovitch, M. Myronov, and A. Ulyanekov, *J. Appl. Phys.* **122**, 105302 (2017).
 - [17] M. Albrecht, S. Christiansen, J. Michler, W. Dorsch, H. P. Strunk, P. O. Hansson, and E. Bauser, *Appl. Phys. Lett.* **67**, 1232 (1995).
 - [18] F. Jonsdottir and L. Freund, *Mech. Mater.* **20**, 337 (1995).
 - [19] M. H. Zoellner, M. I. Richard, G. A. Chahine, P. Zaumseil, C. Reich, G. Capellini, F. Montalenti, A. Marzegalli, Y. H. Xie, T. U. Schüllli, M. Häberlen, P. Storck, and T. Schroeder, *ACS Appl. Mater. Interfaces* **7**, 9031 (2015).
 - [20] F. Rovaris, R. Bergamaschini, and F. Montalenti, *Phys. Rev. B* **94**, 205304 (2016).
 - [21] W. W. Mullins, *J. Appl. Phys.* **28**, 333 (1957).
 - [22] G.-H. Lu and F. Liu, *Phys. Rev. Lett.* **94**, 176103 (2005).
 - [23] J. D. Eshelby, *Proc. R. Soc. A* **241**, 376 (1957).
 - [24] J. P. Hirth and J. Lothe, *Theory of Dislocations*, 2nd ed. (Krieger, Malabar, FL, 1982).
 - [25] F. Rovaris, M. H. Zoellner, P. Zaumseil, M. A. Schubert, A. Marzegalli, L. Di Gaspare, M. De Seta, T. Schroeder,

- P. Storck, G. Schwalb, C. Richter, T. U. Schülli, G. Capellini, and F. Montalenti, [Phys. Rev. Appl. **10**, 054067 \(2018\)](#).
- [26] In order to compare the (2D) experimental results with our (1+1D) simulations we averaged the AFM data of Fig. 1 along one of the two equivalent $\langle 110 \rangle$ directions in a 30- μm -wide region, including about 20 CHP wavelengths for the thinner epilayer and 10 CHP wavelengths for the thicker one. The rms values obtained after this procedure are indicated in the text as $\text{rms}_{2\text{D}}$.
- [27] R. Bergamaschini, M. Salvalaglio, R. Backofen, A. Voigt, and F. Montalenti, [Adv. Phys.: X **1**, 331 \(2016\)](#).